Permission Statement

The report may be cited as:

> Huang, M., Alam, S., Barbour, L. Si, B.C. 2017. Numerical Modelling of the Impact of Cover Thickness on the Long-term Water Balance of Reclamation Soil Covers Over Lean Oil Sands Overburden. Prepared for Syncrude Canada Ltd.

Numerical Modelling of the Impact of Cover Thickness on the Long-term Water Balance of Reclamation Soil Covers over Lean Oil Sands Overburden

Report Prepared For:

Syncrude Canada Limited

Edmonton, Alberta

Report Prepared By:

Mingbin Huang, Shahabul Alam, Lee Barbour

Department of Civil, Geological & Environmental Engineering, University of Saskatchewan

and

Bing Cheng Si

Department of Soil Science, University of Saskatchewan

Date: March 25, 2017

TABLE OF CONTENTS

List of Tables

List of Figures

1 Background and Objectives

Syncrude Canada Ltd. (SCL) is undertaking a watershed scale research program to evaluate the performance of reclamation covers placed over lean oil sands (LOS) at the Fort Hills dump at the Aurora North mine site. This research study is referred to as the Aurora Capping Study (ACS). A key element of the ACS is the assessment of the water balance for alternate cover designs in regard to their adequacy to meet site vegetation growth requirements. Soil-vegetation-atmosphere-transfer (SVAT) numerical modelling has been utilized successfully at other SCL watershed research programs to help with this assessment. In those studies, numerical models were optimized against existing long-term monitoring data (> 10 y) and then used to evaluate long-term (~ 60 y) water balances for alternative cover designs. Recent examples of this approach for South Bison Hill are detailed in the report to SCL by Huang et al. (2012) and in a recent journal paper by Huang et al. (2015). A similar modelling approach was utilized in a preliminary modelling study undertaken during the design of the ACS (Huang et al., 2011); however, that study was based solely on estimated soil properties as no monitoring data was available for calibration. This study undertakes a similar modelling program for the ACS site as that conducted for South Bison Hill. Although the monitoring record is not as long as that available at South Bison Hill, this study is expected to improve our understanding of the performance of the ACS covers relative to the preliminary 2011 modelling study.

The ACS is comprised of a series of 12 alternate cover designs, replicated in triplicate, constructed over the Fort Hills LOS dump at the Aurora mine site. The ACS covers have been monitored over 3 complete growing seasons since their construction in 2012. The existing covers include a range of soil reclamation material types and placement depths, as illustrated in Fig. 1. It is important to note that the LOS characteristics (percent oil, density and texture) are also variable.

SCL has indicated that based on material availability, the final reclamation cover design for the Aurora LOS dumps will likely be a 20 cm peat mixture placed over a sandy subsoil. The key question to be addressed in this study is whether there is an optimal depth of sandy subsoil which will meet the desired revegetation requirements. Consequently, this study will focus on only the peat over subsoil covers at ACS with the following study objectives:

(1) Develop optimized water balance models for existing ACS covers comprised of peat placed over subsoil (Treatments 1, 3), bare subsoil (Treatment 12b), and the peat treatments (Treatment 5);

(2) Simulate the long-term performance of a series of hypothetical covers comprised of a 20 cm peat layer placed over a range of subsoil cover depths (50, 75, 100, 125, 150 cm) to evaluate the impact of the thickness of the subsoil on performance, particularly transpiration and water release.

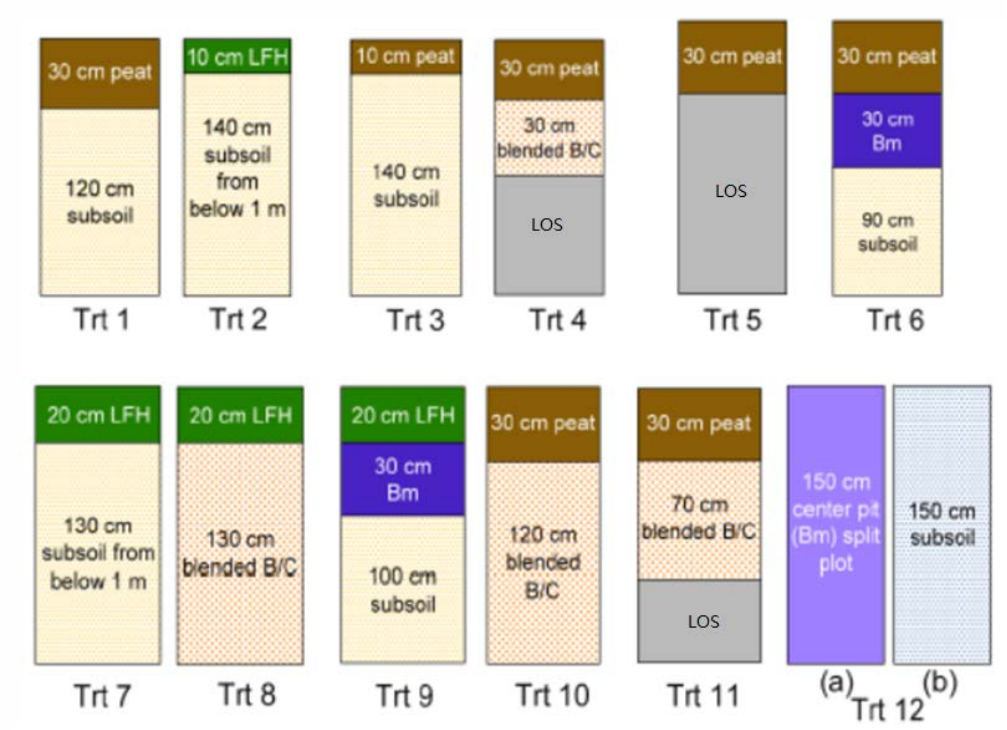

Figure 1. Soil Cover Design Treatments at ACS (O'Kane Consultants, 2015).
Trt refers to the Treatment type number for each cover. LOS underlies all treatments.

2. Materials and Methods

2.1 Covers

Optimized models were developed for four covers: Trt 1, Trt 3, Trt 5, and Trt 12b. The nominal thickness and cover materials used in these covers are illustrated in Fig. 2. The soil cover monitoring cells for each of these covers are as follows: Trt 1 - Cells 9, 33, and 35; Trt 3 – Cells 8, 13, and 29; Trt 5 – Cells 05, 20, and 31; Trt 12b - Cells 19b, 27b, and 36b.

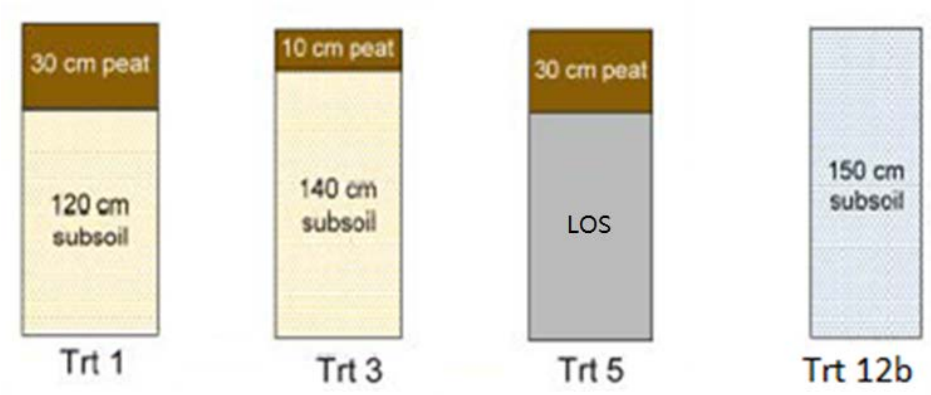

Figure 2. Four cover treatments at ACS selected for model calibration.

Particle size distribution (PSD) analyses of the soil reclamation materials (i.e., peat and subsoil), as well as the surface LOS landform substrate were performed by MDH Engineered Solutions using samples collected by O'Kane Consultants Inc. (OKC, 2009) in November of 2009 (Fig. 3). The standard analysis method of ASTM D422 was used for the PSDs for all materials. The ASTM D422 is based on the assumption of mineral particles which are typically spherical, and consequently the PSD results for peat are likely not representative. Although the PSD of the peat component of the peat mixture is difficult to characterize, it is clear that the subsoil is relatively uniform while the mineral component of the LOS has the greatest textural variability.

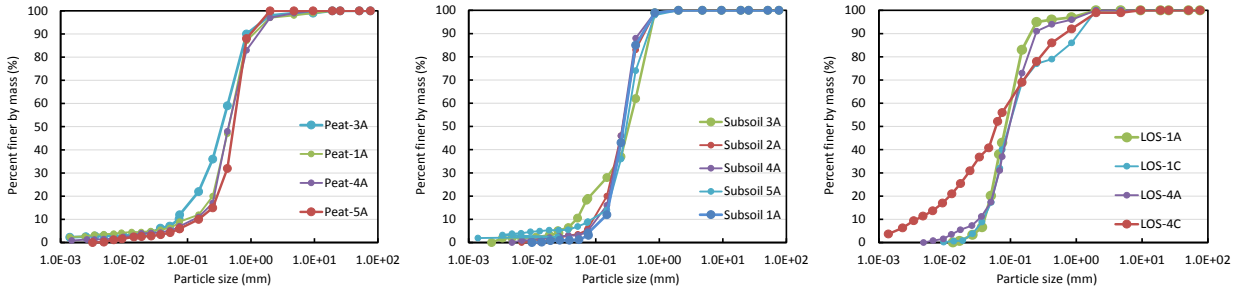

Figure 3. Particle size distribution for peat, subsoil, and LOS (OKC, 2009).

2.2 Field measurements

Field monitoring at the study cells has been ongoing since 2012. Depth profiles of soil suction, temperature and volumetric water content are monitored across the cover and into the underlying LOS at one location within in each cell. Tank and Gee lysimeter monitoring is available at a smaller number of cells. Climate monitoring data (wind speed, relative humidity, net

radiation, and precipitation) is also available from one location on the ACS. All ACS monitoring data was obtained from O'Kane Consultants and is summarized, along with preliminary interpretations of water balance, in annual reports including OKC (2014, 2015, 2016). O'Kane Consultants also provided assistance in interpreting the monitoring data.

Tree planting plots were established for all treatments. At each cell there were four plots (25 × 25 m), each with one of four vegetation treatments: single species plots with trembling aspen (*Populus tremuloides* Michx.), jack pine (*Pinus banksiana* Lamb), white spruce (*Picea glauca* (Moench) Voss), and a plot with an even mix of all three species. All plots were planted in the spring of 2012 with one-year-old containerized planting stock at a 1 × 1 m spacing.

The LAI of each treatment was estimated (qualitatively) for the calibration simulations using recent photographs of above-ground vegetation growth. The peak season LAI values varied from 0.1 at Trt 12b to 0.8 at Trt 3. The seasonal variation of LAI was simplified for the calibration modelling as shown in Fig. 4.

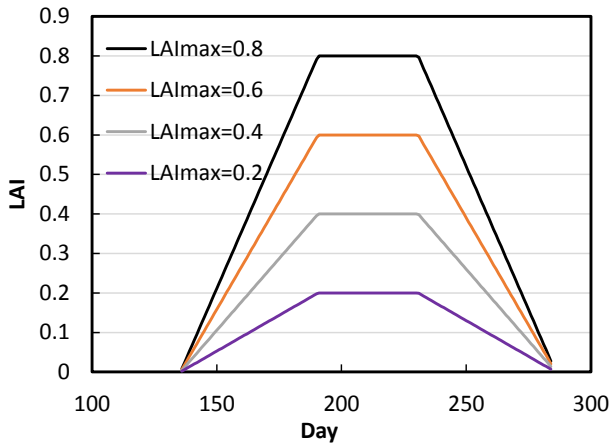

Figure 4. Variations of four special LAI values in growing season.

The root distribution for the calibration models were estimated based on measurements provided by Bockstette et al (2016) for Trt 1 and 5 (Fig. 5). The maximum root depth was assumed to be 0.3 m at Trt 5 and 0.5 m at Trt 1, 3, and 12b. An exponential rooting distribution with depth was assumed for each treatment as shown in Fig. 6.

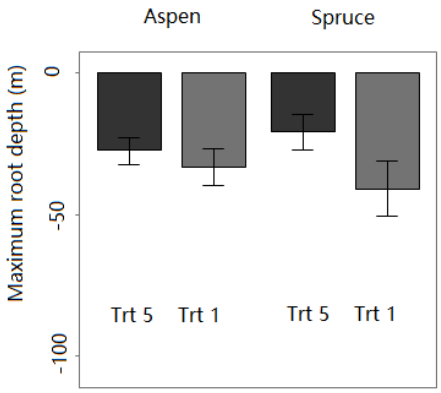

Figure 5. The maximum root depths for Trt 1 and Trt 5 (Bockstette et al., 2016).

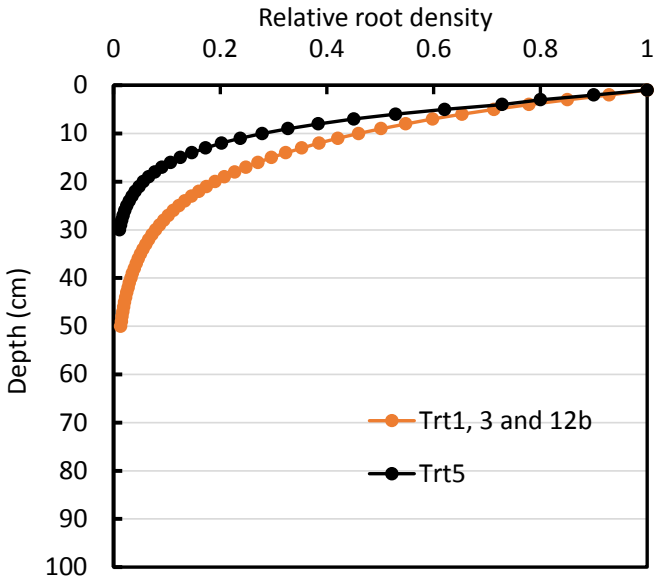

Figure 6. Root distribution of each treatment.

2.3 Numerical model

The same numerical model was used for both the calibration and optimization simulations. However, in the case of the calibration model, the vegetation characteristics (i.e. LAI, root depth) were estimated from field observations, while in the optimization simulations it was assumed that the vegetation had reached maturity. The description of the modelling approach used for the calibration is described in the following sections and the long-term optimization simulations are described in Section 2.4.

2.3.1 Governing equation

A single-porosity model for water flow was used to describe water movement with root uptake water:

$$\frac{\partial \theta}{\partial t} = \frac{\partial}{\partial z}[K(h)(\frac{\partial h}{\partial z} + 1)] - S_r \quad [1]$$

where Θ and h are the volumetric water content [$L^3\ L^{-3}$] and pressure head [L], respectively, and S_r is the root uptake rate [$L^3\ L^{-3}\ T^{-1}$].

The unsaturated hydraulic properties for the pores were described using the van Genuchten-Mualem equations (1980):

$$\theta(h) = \begin{cases} \theta_r + \dfrac{\theta_s - \theta_r}{[1 + |\alpha h|^n]^m} & h < 0 \\ \theta_s & h \geq 0 \end{cases} \quad [2]$$

$$K(h) = \begin{cases} K_s S_e^{1/2}[1 - (1 - S_e^{1/m})^m]^2 & h < 0 \\ K_s & h \geq 0 \end{cases} \quad [3]$$

$$S_e = \frac{\theta - \theta_r}{\theta_s - \theta_r} \quad [4]$$

where S_e is the effective degree of saturation[$L^3\ L^{-3}$] and subscripts *r* and *s* refer to residual and saturated conditions, respectively; α[L^{-1}], *n*, and *m* are van Genuchten (VG) equation parameters, and m=1-1/n; and K_s is the saturated hydraulic conductivity [$L\ T^{-1}$].

2.3.2 Root water uptake

The root uptake (sink) term in Eq. [1] represents the potential transpiration rate (T_p) reduced by a factor which represents that rate at which soil can supply water to roots ($\alpha(h)$) and the root distribution function (b(z)). The HYDRUS-1D model incorporates these relationships and results in a root water uptake function as follows (Feddes et al. 1974):

$$S(h) = \alpha(h)\frac{b(i)}{\sum_{i=1}^{\ell} b(i)} T_p \quad [5]$$

where $\alpha(h)$ is the root water uptake stress response function. Eastman and Camm (1995), Dang et al. (1997), and Kimball et al. (1997) found that the discrete function based on two pressure heads was effective for white spruce and trembling aspen as follows:

$$\alpha(h) = \begin{cases} 1, & h \geq h_1 \\ \dfrac{h_2 - h}{h_2 - h_1}, & h_2 < h < h_1 \\ 0, & h \leq h_2 \end{cases} \quad [6]$$

The two pressure heads (h_1 and h_2) were based on previous studies reported in the literature. For White Spruce, the reported value was 500 and 1,500 kPa for h_1 and h_2, respectively (Eastman and Camm, 1995), and 500 and 2,300 kPa, respectively, for trembling aspen (Bond-Lamberty et al., 2005; Kimball et al., 1997). In this study, the average values of 500 kPa and 1,900 kPa for h_1 and h_2, respectively, were used in all models.

2.3.3 Partitioning of potential evaporation and transpiration

The daily potential evapotranspiration (PET), calculated using the Penman-Monteith equation, is partitioned into potential soil evaporation (PSE) and potential plant transpiration (PPT) using the leaf area index (LAI) as follows:

$$PPT = PET(1 - e^{-\mu LAI}) \quad [7]$$

$$PSE = PETe^{-\mu LAI} \quad [8]$$

where μ is an empirical parameter varying from 0.50-0.75 for trees (Ritchie 1972). In this study, an average value of 0.62 was used for partitioning PET into PSE and PPT from LAI (Fig. 4). It is important to note that the relatively small LAI values assumed for the Treatment plots for the calibration study tends to result in more partitioning of PET into PSE, while the assumed mature LAI values used in the long-term modelling would tend to partition more PET into PPT.

2.3.4 Rainfall Interception

In HYDRUS-1D, Braden's (1985) equation is used for interception estimation:

$$I = aLAI\left(1 - \frac{1}{1 + \frac{bP}{aLAI}}\right) \quad [9]$$

$$b = 1 - e^{-\mu LAI} \quad [10]$$

where I is the rainfall interception, P is rainfall, and a is a parameter equal to 0.25 mm, similar to the agricultural crops (van Dam et al., 1997). There was not a readily available value for trees, and given the lack of tree growth during the early years at the site, the literature value was assumed.

2.3.5 Model Domain

A one-dimensional model domain which included 100 cm of LOS overlain by the selected cover thicknesses was used to represent each cell. As a result, the total thickness of each model was as follows: 250-cm for Trt 1 (consisting of 30 cm peat, 120 cm subsoil and 100 cm LOS), Trt 3 (consisting of 10 cm peat, 140 cm subsoil and 100 cm LOS), and Trt 12b (consisting of 150 cm subsoil and 100 cm LOS); and Trt 5 (consisting of 30 cm and 220 cm LOS). The spatial discretization was 1 cm for all model domains.

2.3.6 Initial and boundary conditions

Only the days in which the cover was unfrozen were simulated. In the optimization models, it was assumed that snowmelt was complete prior to ground thaw and consequently any changes in soil water storage as a result of snow melt were assumed to be represented in the water content profiles from the first day in which the cover was unfrozen (i.e. soil temperatures > 0^{o}C). The measured volumetric water content profile on the first unfrozen day was used as the initial condition. A unit gradient was set as the lower boundary of the domain. The upper boundary condition was represented by soil-vegetation-atmosphere-transfer (SVAT) parameters (e.g. climate and vegetation characteristics).

2.3.7 Parameter calibration

The inverse solution sub-program in HYDRUS-1D was used to optimize the hydraulic parameters of the peat, subsoil and LOS. The parameters were optimized independently for each cell and each year of monitoring using the observed soil moisture data. For the single porosity model, five parameters are optimized for each soil type (Θ_r, Θ_s, α, n, and K_s). The Θ_r was constrained by values between 0 and the measured minimum water contents within the cover, while Θ_s was constrained by the estimated porosity and the measured maximum water content. The α, n, and K_s were only weakly constrained to be within a realistic range based on soil texture and literature values (Pernitsky et al., 2016; Sigouin et al., 2016).

2.3.8 Uncertainty of the estimated hydraulic parameters

The uncertainty of the hydraulic parameters for the 3 materials (peat, subsoil and LOS) was evaluated in two ways: (1) by evaluating the range (uncertainty) in all optimized model parameters obtained for different cells in all years; and (2) by evaluating the range (uncertainty) in the mean of model parameters obtained for different cells in all years. The first way provides a parameter set that represents the overall parameter uncertainty, while the second way represents only spatial uncertainty. The overall parameter uncertainty would include both spatial and temporal uncertainties. Temporal uncertainty can develop as a result of the evolution of the cover properties over time, as observed at the 30D study site (Meiers et al., 2011). Even without actual temporal parameter evolution, variations in the optimized parameters with time could occur due to the differences in the range of observed water content variations from one year to the next. The parameter variability captured in the overall parameter uncertainty is mostly likely due to variability associated with material heterogeneity (e.g. texture or LOS bitumen content) and differences in placement conditions (compaction and texture, cover thickness). The only independent check made on this variability was to compare the results from the calibration to direct measurements of field saturated hydraulic conductivity (K_s). This comparison is provided in a discussion of the results in Section 3.5

2.4. The long-term simulations

The long-term performance of the hypothetical covers (i.e. varying subsoil thickness) were simulated using the distribution of optimized model parameters and with 60 years of climate data available from the Fort McMurray airport weather station. Although computationally intensive, this approach allows the uncertainty in optimized model parameters to be reflected in the long-term water balance simulations.

2.4.1 Five hypothetical covers

The hypothetical covers were assumed to have a 20 cm peat layer and a range of subsoil cover depths (50, 75, 100, 125, 150 cm) as shown in Fig. 7.

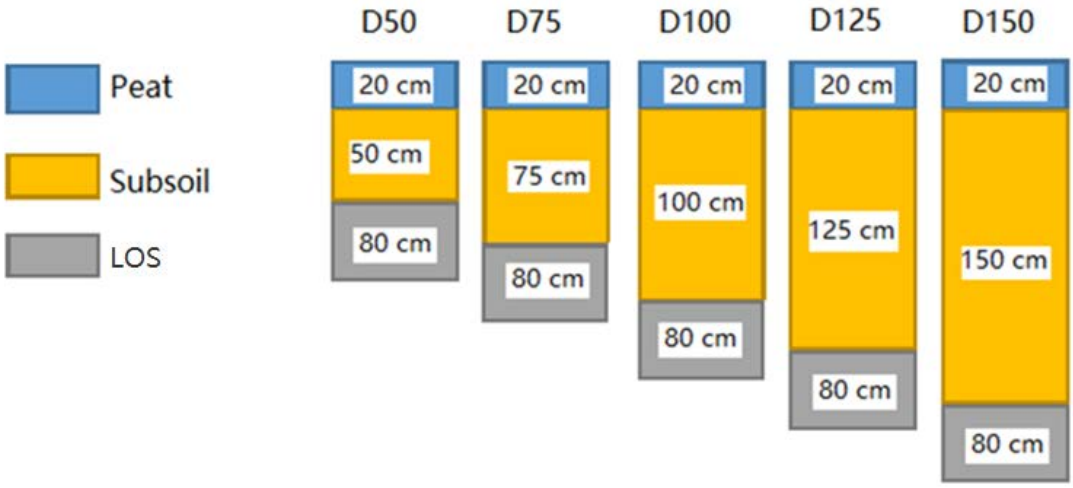

Figure 7. Five modelled hypothetical covers.

2.4.2 The long-term climatic data

The long-term climate data was the 1952-2013 data from the Fort McMurray airport weather station (e.g. maximum and minimum air temperature, relative humidity, wind speed, dew temperature, sunshine hours, and precipitation). Table 1 provides a statistical summary of this data. The Penman-Monteith equation (Allen et al., 1998) was used to calculate daily PET. The simulations were conducted only for unfrozen conditions (i.e. growing season). Precipitation falling as snowfall, minus an assumed annual sublimation, was accumulated during the winter

period. The annual sublimation was assumed to be represented by the difference in the measured values of precipitation as snow from the Fort McMurray airport weather station (FMAWS), and the measured values of snow water equivalent (SWE) obtained from snow surveys at SBH for years in which snow survey data was available. During the period of 2003 to 2011, the average relative difference was 7.1%. The total snowpack volume was applied to the covers as infiltration during the first week of spring when the soil cover was unfrozen.

Repeated simulations of the 1952-1953 climate data was used to spin up the model and establish the initial conditions for the long-term simulation (i.e. 1954 to 2013).

Table 1. Mean and standard deviation (STD) for climatic variables from 1952 to 2013.

	Annual Rainfall (mm)	**Annual SWE (mm)**	**Daily max. T (°C)**	**Daily min. T(°C)**	**Daily relative humidity (%)**	**Daily average wind speed (Km/day)**	**PET (mm)**	**Daily sunshine (hour)**
Mean	312.7	130.5	6.6	-5.6	70.1	231.7	496	5.7
STD	80.6	42.4	15.0	13.8	13.5	107.1	52	2.6

2.4.3 Vegetation cover scenarios

The numerical model requires a specified pattern of seasonal variations in LAI. In order to check that the specified values of LAI used in the model were consistent with simulated transpiration rates, six seasonal patterns of LAI were used to simulate each cover (Fig. 8). The AET generated from each of these cases were then used to estimate the maximum sustainable LAI for the hypothetical covers as discussed in Section 3.9.

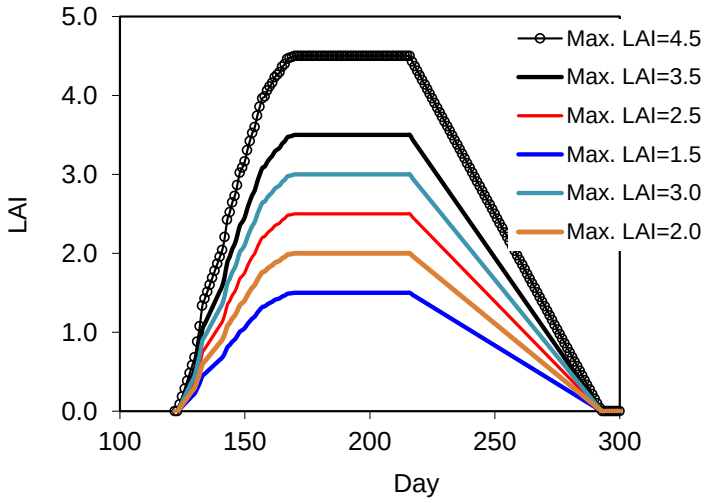

Figure 8. Assumed LAI values and their variation during the growing season.

A simple exponential root system distribution was assumed to be fully developed within the peat and subsoil; however, it was assumed that roots did not penetrate into the LOS (Fig. 9). This assumption may be overly conservative (i.e. under-estimation of rooting depth and available soil water storage) and may need to be reconsidered in the future as additional information on plant performance becomes available.

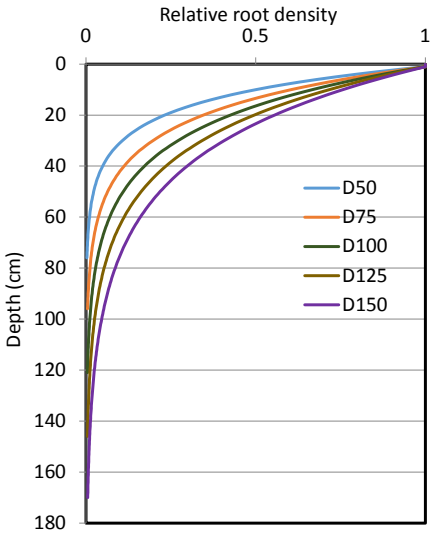

Figure 9. The exponential root system distribution for each cover.

2.4.4 Boundary conditions

A unit gradient was applied to the lower boundary of the domain. The SVAT boundary conditions (e.g. climate and vegetation) described previously were applied to the upper boundary of the model.

2.4.5 Uncertainty of the simulated T_r and NP for each cover scenario

The WRC and K_s for each soil type in the model was selected from the distributions obtained from the parameter optimization modelling. Rather than attempt a full Monte Carlo type simulation (i.e. random selection) a sensitivity type approach was used to capture the variability in the input properties. Three alternate WRCs, representing the median, 90 percentile, and 10 percentile of the optimized parameters, were used for the Peat, while only the median WRC was used for the Subsoil and LOS. Three K_s values (the median, 10 percentile, and 90 percentile) were used for the peat and subsoil along with five different K_s values (95, 75, 50, 25, 5 percentiles) for the LOS. All of these various combinations were simulated for each of five hypothetical covers, with repeat simulations for each of the six different prescribed LAI values. This results in a total of 135 combinations of properties for each cover scenario (i.e. 3 Peat WRCs x 3 Peat K_s values x 1 Subsoil and LOS WRC x 3 Peat K_s values x 3 Subsoil K_s values x 5 K_s values). Each combination of properties was simulated for 60 years for each value of LAI and for each cover type (i.e. total number of simulations equal to 4050). The simulated distributions of annual T_r (actual transpiration) and NP (net percolation) for each cover scenario with each LAI value were calculated from 60 years with 135 realizations.

2.5 Statistical analyses

The Student's T test was used to exam the normal distribution for each of five hydraulic parameters as obtained from the parameter optimization at all cells and all years. The parameters of Θ_r, Θ_s, α, and n were normally distributed while the K_s was log normally distributed. A log normal distribution for K_s is commonly observed in the literature. The mean, standard deviation (STD) and coefficient of variation (CV) were calculated for Θ_r, Θ_s, α, n, and Log(K_s) and consequently used to compare the distributions of the combined set of optimized material properties (all locations, all

years) with the optimized properties for each individual cell for the combined 3 years. The CV was used as an index of the uncertainty in the hydraulic properties – a larger CV implying greater uncertainty. The CV value for the overall uncertainty (all cells, all years) reflects overall uncertainty while the CV for the combined mean values from individual cells reflects only spatial variability (assuming limited temporal evolution has occurred in individual cells).

3. Results and Discussion

3.1 Comparison of the measured and simulated water contents for each treatment

The simulated and observed water contents were in good agreement (Fig. 10). Linear regressions of the simulated verses observed water contents for all locations had R^2 values of 0.85 to 0.95, slopes from 0.86 to 0.97, and relatively small intercepts (0.006 to 0.050 cm^3/cm^3) with root mean square root (RMSE) from 0.023 to 0.047 cm^3/cm^3. Generally, the largest differences between measured and simulated values occurred for the shallow, 5 cm depth at Trt 3. The measured water contents at these locations may be more subject to errors due their shallow depth and the potential for the sensors to become exposed as a results of sediment loss. Cell 13 at Trt 3 was not used for calibration due to unreasonable soil water measurements in the peat.

3.2 Comparison of the measured and simulated net percolation rates for Cells 29 and 33

The net percolation (NP) from the base of the model was compared to the measured NP rates observed in selected Tank lysimeters. The net percolation rates were simulated using a 300-cm domain with the specific hydraulic parameters optimized in each year at each cell. A 10 cm sand layer was placed below the LOS in these simulations and the lower boundary was set to be a free drainage boundary.

O'Kane Consultants (OKC, 2015) have noted difficulties with the performance of Tank lysimeters. There were 3 tank lysimeters at the treatments for this study (i.e. there was no tank lysimeter installed at Trt 12b). O'Kane Consultants suggested that the results from Tank lysimeter Cell 29 in 2014 and 2015 and from Tank lysimeter Cell 33 in 2013-2015 were reliable, while the NP values from the lysimeter in Cell 31 was consistently high through all years. The NP from the tank lysimeter installed in Cell 31 was not used for comparison.

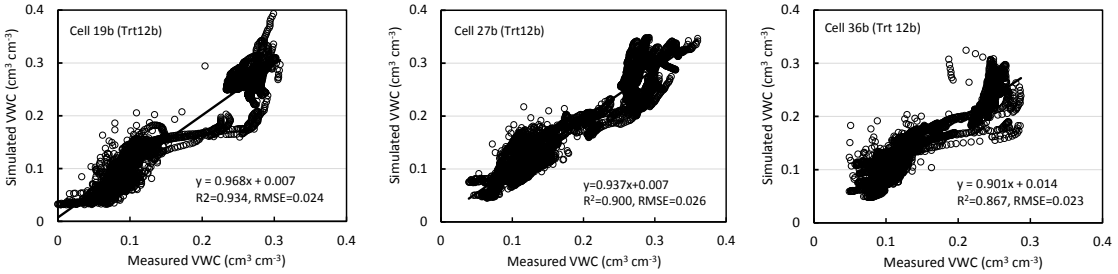

a) Cells 19b, 27b, and 36b at Trt 12b.

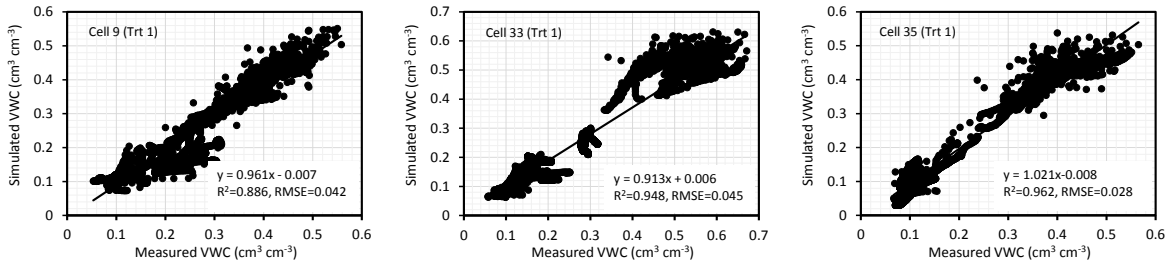

b) Cells 9, 33, and 35 at Trt 1.

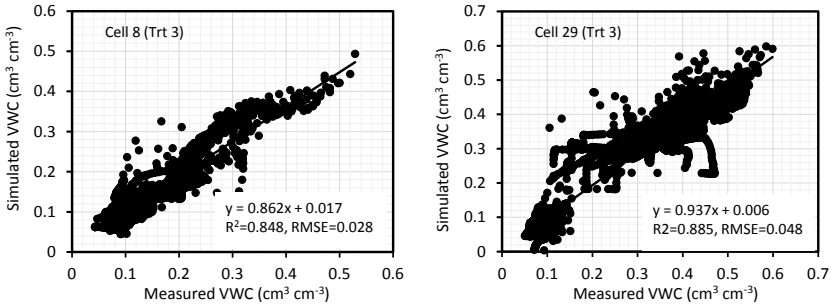

c) Cells 8 and 29 at Trt 3.

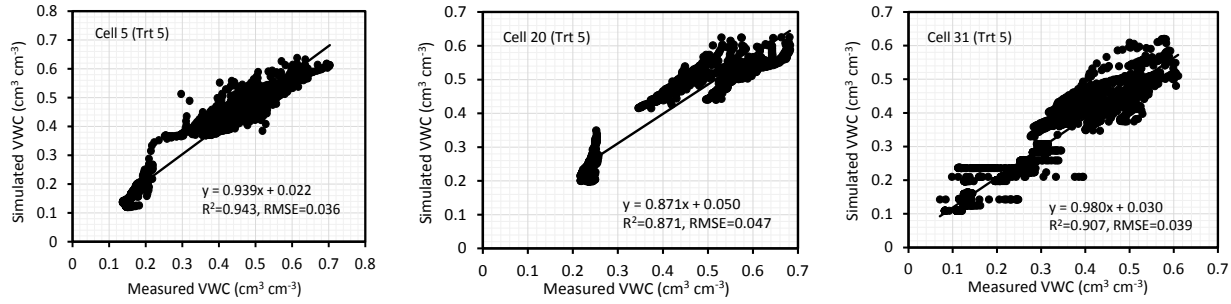

d) Cells 5, 20 and 31 at Trt 5

Figure 10. Comparison of the measured and simulated water contents.

There is similar pattern of cumulative NP for the measured and simulated Cell 33 (2014 and 2015) and Cell 29 (2015) cases (Fig. 11). The model overestimated the NP in 2013 for Cell 33 and underestimated the NP in 2014 for Cell 29.

The four Gee lysimeters installed in Cells 29 and 33 did not show reasonable NP responses and consequently were not used for comparison purposes.

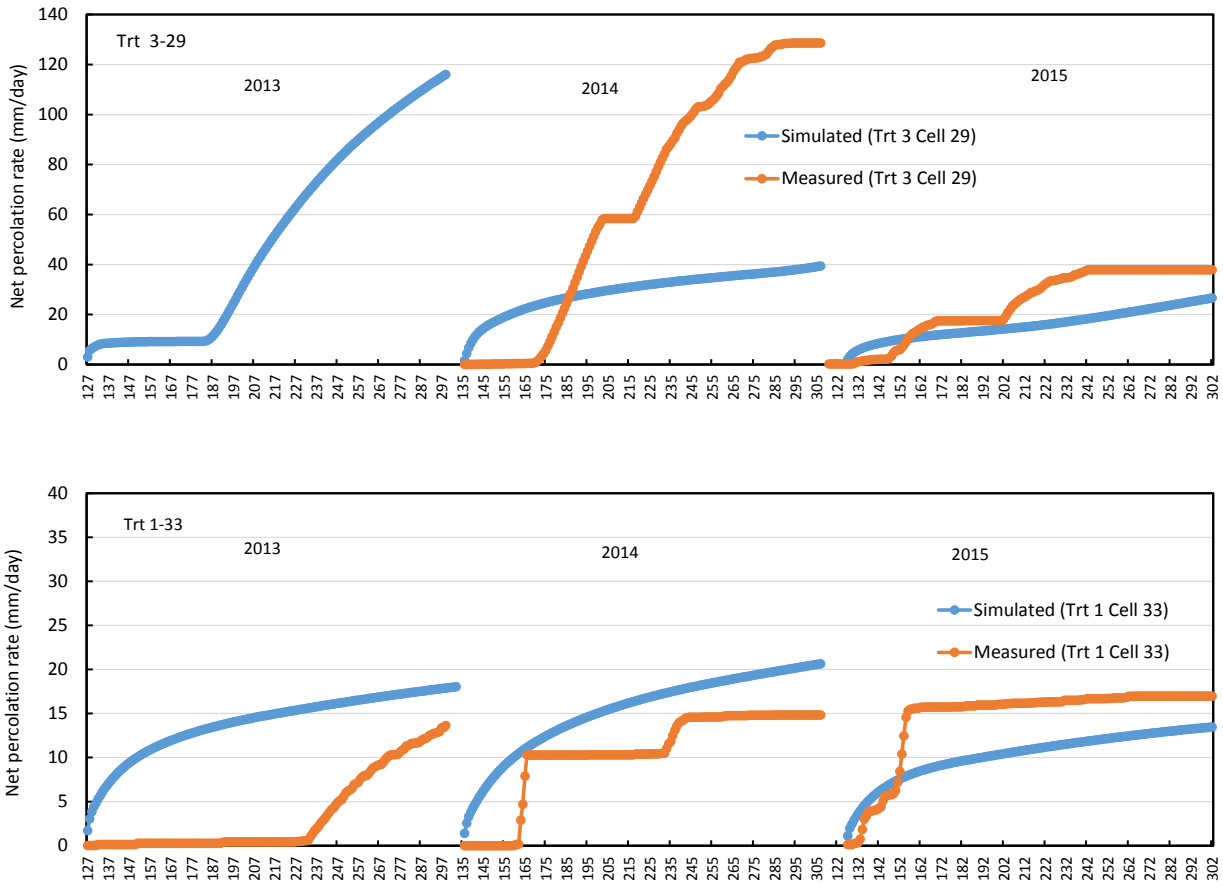

Figure 11. Comparison of the measured and simulated net percolation (NP) rates for Cells 29 and 33.

3.3 Optimized hydraulic properties and uncertainty for all cells

Table 2 summarizes the mean, STD, and CV of each hydraulic parameter for each material using the optimized properties from all cells and years. These STD and CV values represent the overall material property variability. The range in overall variability among five parameters was in the following order (of decreasing variability): $K_s > \Theta_r > \alpha > n > \Theta_s$ for the peat; while, for subsoil and LOS, this order varied as $K_s > \Theta_r > \alpha > \Theta_s > n$ (Table 2). This result is not surprising since K_s is known to be a highly variable material property. The high CV values for Θ_r of the subsoil is likely due to the low values for Θ_r in such a coarse–textured material. The optimized Θ_r ranged from 0 to 0.060 cm^3/cm^3.

When comparing the three different materials, it is apparent that the LOS had the greatest material property variability. This is due fundamentally to the natural geologic variability, as well as variability in placement conditions (e.g. compaction). However, it may also be accentuated by the following: (1) the LOS had the smallest number of water content monitoring points against which to calibrate; (2) the measured soil water contents in the LOS varied over a relatively small range and were not strongly affected by surface evaporation or root water uptake.

Table 3 summarizes the mean, STD, and CV of each hydraulic parameter calculated using the mean of each hydraulic parameter at each cell. These STD and CV values only represents the spatial uncertainty of each hydraulic parameter. In general, site to site variability (i.e. spatial variability) contributed to approximately 86% of the overall parameter uncertainty for K_s (Fig. 12). This would suggest that variability in K_s will exert a primary influence in the water balance modelling. Because the parameters of Θ_r, Θ_s, α, and n are not independent, the uncertainty of soil water retention curve (SWRC) cannot be determined by their STD and CV values.

Table 2. The mean, standard deviation (STD), and coefficient of variation (CV) of each hydraulic parameter using all optimized values at all cells for each material.

Soil	Θ_r (cm^3/cm^3)			Θ_s (cm^3/cm^3)			α (1/cm)			n			Log (K_s) (cm/d)		
	Mean	STD	CV	Mean	STD	CV	Mean	STD	CV	Mean	STD	CV	Mean	STD	CV
Peat	0.047	0.027	57.6	0.592	0.053	8.9	0.049	0.018	36.2	1.164	0.105	9.0	-4.74	0.34	-7.2
Subsoil	0.015	0.019	124.6	0.367	0.038	10.4	0.028	0.007	24.4	2.095	0.202	9.7	-4.67	0.35	-7.5
LOS	0.065	0.036	55.1	0.385	0.052	13.4	0.041	0.009	20.6	1.825	0.206	11.3	-6.79	0.76	-11.2

Table 3. The mean, standard deviation (STD), and coefficient of variation (CV) of each hydraulic parameter calculated using the mean at each cell for the same material.

Soil	Θ_r (cm^3/cm^3)			Θ_s (cm^3/cm^3)			α (1/cm)			n			Log (K_s) (cm/d)		
	Mean	STD	CV	Mean	STD	CV	Mean	STD	CV	Mean	STD	CV	Mean	STD	CV
Peat	0.047	0.019	41.1	0.592	0.050	8.5	0.049	0.015	30.3	1.165	0.085	7.3	-4.69	0.28	-6.0
Subsoil	0.015	0.015	98.2	0.367	0.036	9.7	0.028	0.007	23.6	2.095	0.194	9.2	-4.60	0.34	-7.3
LOS	0.065	0.031	47.0	0.385	0.042	11.0	0.041	0.007	17.6	1.825	0.188	10.3	-6.60	0.58	-8.8

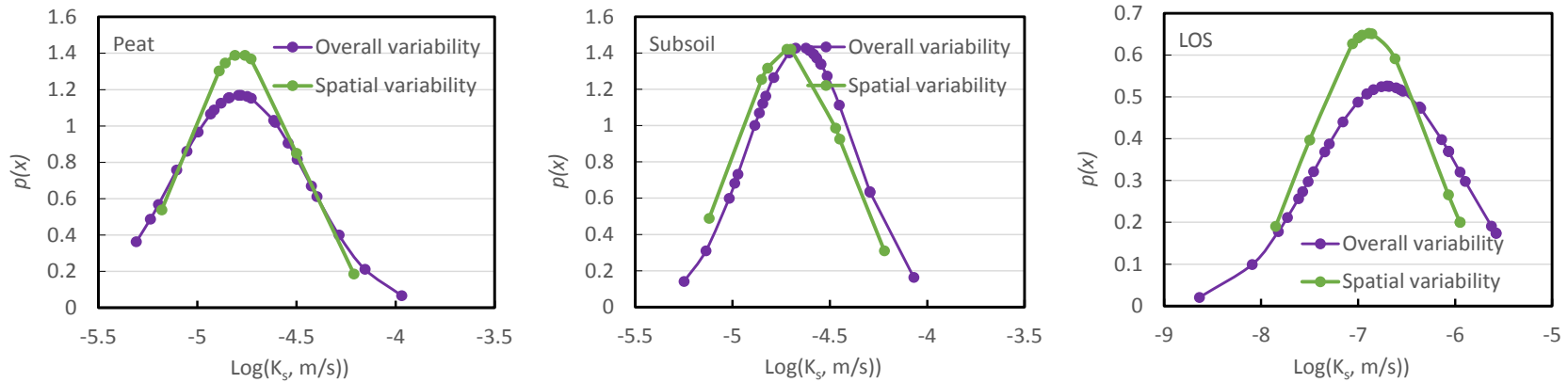

Figure 12. The probability distributions of Ks overall variability and spatial variability for each material.

3.4 Spatial variation of optimized SWRC and K_s

Fig. 13 shows the envelope of optimized WRCs for each material at all sites and all years as defined by the median, 10th and 90th percentile values. The distribution of the optimized K_s values are presented in Fig. 14. In the case of K_s, the variation in optimized K_s values can be compared to the variation of K_s from the direct field measurements made using the Guelph (K_{fs}) and air ($K_{s\text{-}a}$) permeameters (OKC, 2013). The values of K_s are not expected to correlate directly to optimized K_s values, particularly in the case of $K_{s\text{-}a}$ (Huang et al., 2016). However, the similar shapes of the optimized and measured Ks distributions indicate that these independent measures of variability are similar. Among three material types, the peat appears to show the largest variability in WRC; whereas the LOS showed the largest uncertainty in K_s estimation (Table 2).

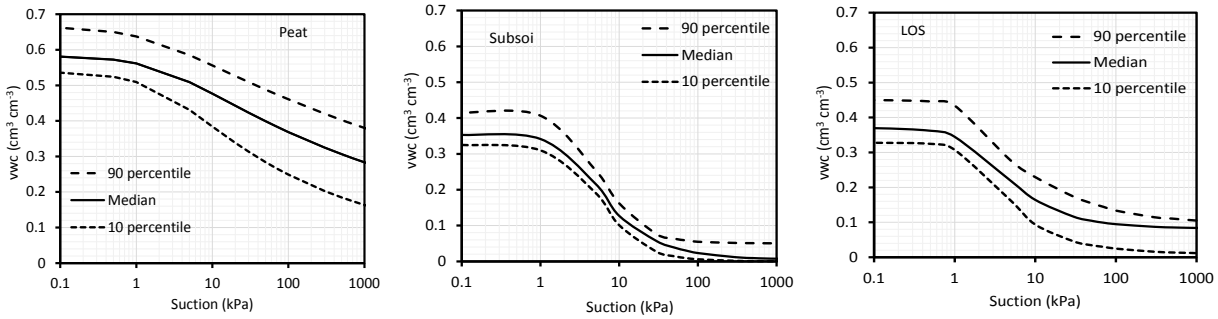

Figure 13. Uncertainty of estimated soil water retention curves for each material type.

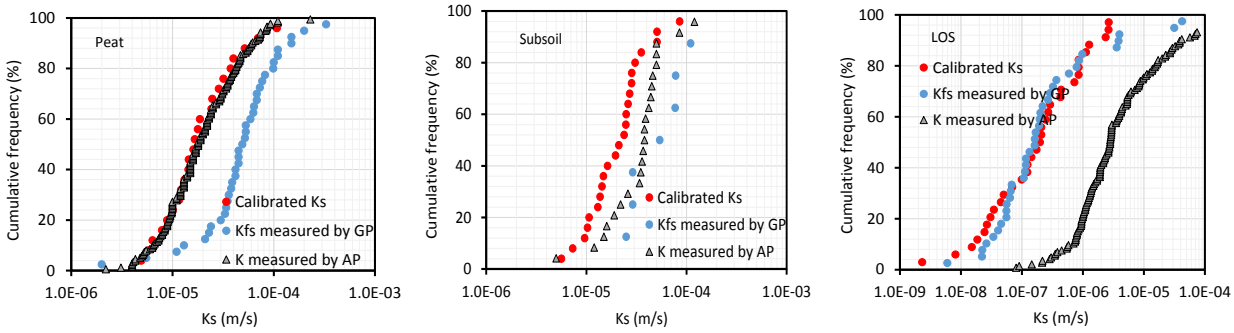

Figure 14. The distributions of optimized Ks, measured field saturated Kfs using Guelph permeameter and Ks using Air permeameter for peat, subsoil, and LOS by OKC (OKC, 2013).

The K_s values for LOS had the largest range among the three materials. This is not unexpected given the geological variability in the LOS and the associated variability in bitumen content, as well as variations in compaction. The measured bitumen content ranged from 0.2 to 6.9% in the LOS, whereas the bulk density varied from 1.22 to 1.82 g/cm^3 (Zettl et al., 2014)

The optimized K_s values for peat and subsoil were less than those measured using a Guelph permeameter; however, they were within the same order of magnitude as the field measured values. The optimized K_s values for subsoil and LOS were less than those measured using an air permeameter as discussed by Huang et al. (2016), however the optimized K_s values for peat were very similar to the values measured using an air permeameter. The optimized K_s values for LOS were also very similar to the values measured using the Guelph permeameter. The optimized K_s values within 9 cells are plotted against the measured $K_{s\text{-}a}$ from the same nine cells in Fig. 15. No significant linear relationship was found between the K_s values obtained using different methods, although they had similar probability distributions. This suggests that the variation in the LOS K_s was occurring at a spatial scale less than the size of an individual cell.

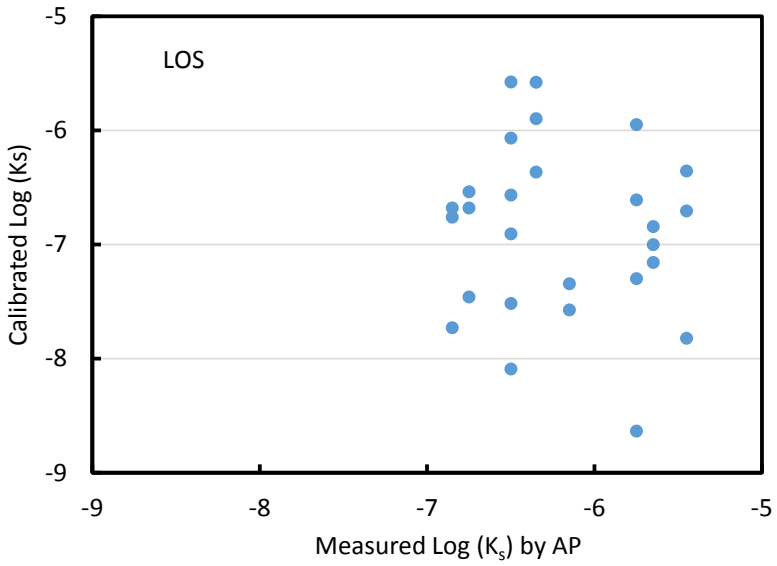

Figure 15. The optimized Ks vs. the measured Ks using air permeameter for LOS at 9 cells.

3.5 T_r Frequency Distribution and Uncertainty for Long-Term Simulation

Fig. 16 shows a typical set of the 135 frequency distributions for 60 years of annual T_r from the long-term simulations. This case was for the D100 cover with a LAI of 3.0. The finer lines represent each individual simulation result (i.e. annual T_r distribution for 60 year model) and the heavier lines show the 10th, 50th, and 90th percentiles for the entire frequency distributions. Similar plots of the 10th, 50th and 90th percentiles for annual T_r obtained in simulations of the alternative covers for LAI values of 1.5, 3 and 4.5 are presented in Fig. 17. These figures illustrate that although LAI (assumed) has a strong influence on annual T_r, there is little variation in the annual T_r distribution as a result of changes in subsoil layer thickness.

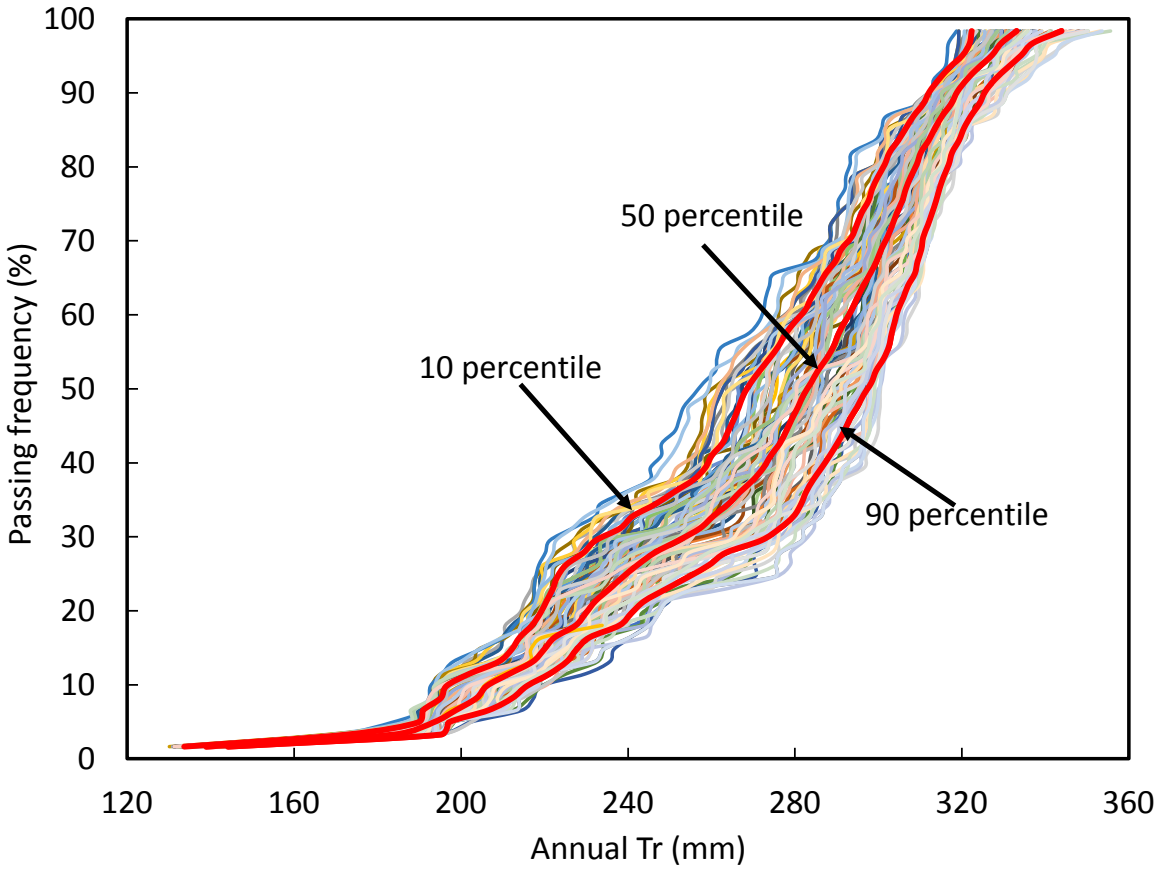

Figure 16. The frequency distribution of annual T_r at 135 realizations for the D100 cover with an LAI of 3.0.

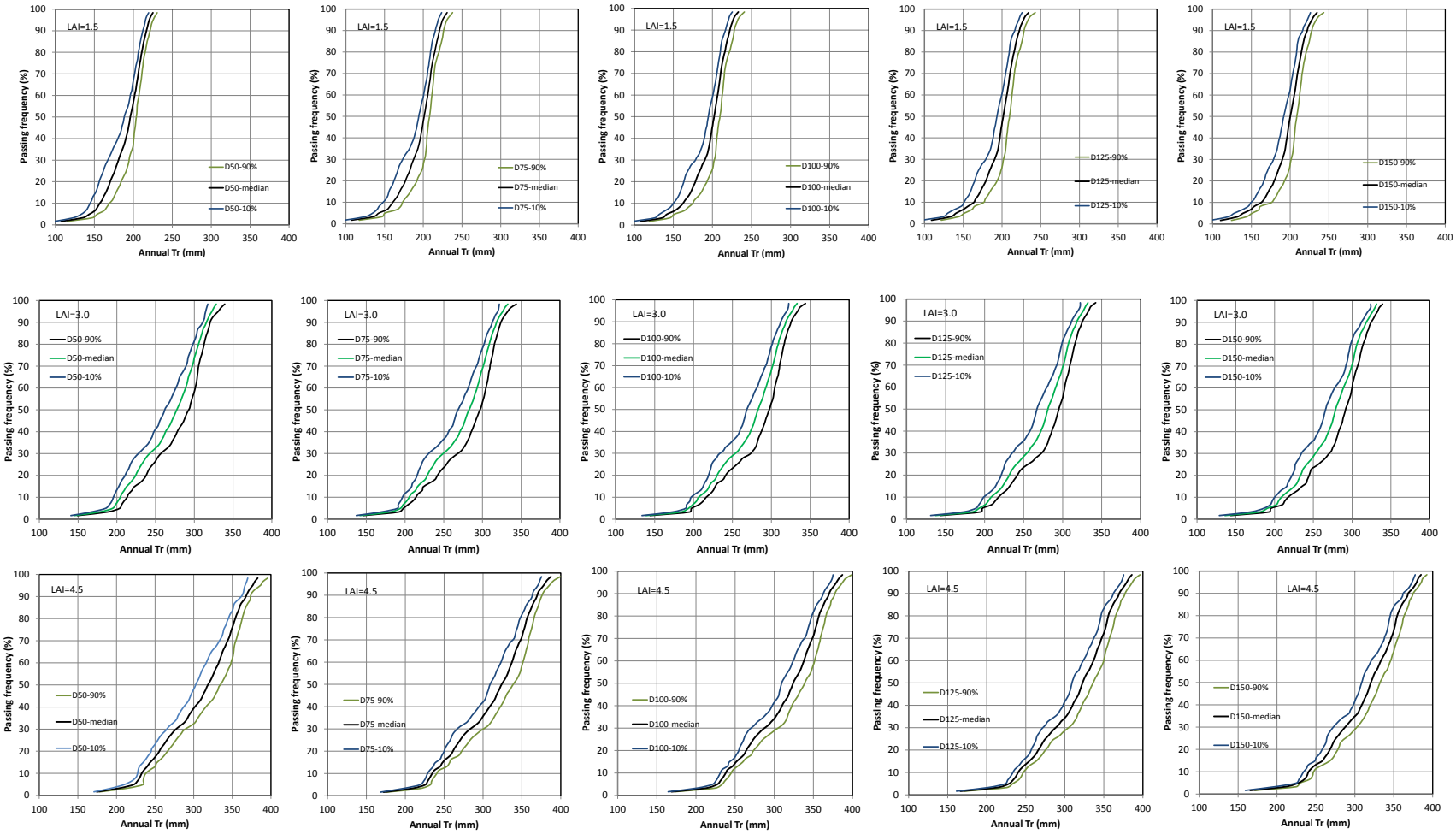

Figure 17. The frequency distribution and uncertainty of annual T_r at the 10th, 50th, and 90th percentiles for each covers with the LAI=1.5, 3.0, and 4.5. The D50, D75, D100, D125 and D150 represent the subsoil thicknesses of 50, 75, 100, 125 and 150 cm, respectively.

The controls on annual T_r are more effectively illustrated through the use of a sensitivity analyses in which the median annual T_r values from a base case of fixed LAI (3.0), subsoil thickness (100 cm), and median values of LOS K_s, peat K_s, and peat storage are compared to cases in which only one of the other parameters are varied. For example, additional simulations were run using either a maximum or minimum value of LAI, a maximum or minimum thickness, and the 10^{th} or 90^{th} percentile of the hydraulic properties (Table 4). The result of this simulation is referred to as a Tornado plot (Fig. 18) in which the factors which produce the greatest range of T_r values are plotted above those which have less influence on T_r. It is clear that LAI had the biggest influence on T_r followed by LOS K_s and peat K_s. The subsoil cover thickness only had a moderate influence on annual T_r. The variation of LAI used in the simulation is arbitrary and may not be consistent with the simulated T_r. This will be discussed further in Section 3.9. The control exerted by the LOS K_s is thought to be due to the fact that low values of LOS K_s will restrict drainage of the soil profile, thereby increasing water available in the soil cover that can be used by vegetation. The influence of peat K_s appears to be due to the fact that higher values of peat K_s will move more water to the surface where it can be evaporated, and consequently, higher values of peat K_s actually result in lower values of T_r since more of the available water is lost through surface evaporation.

Table 4. The mean, and 10^{th} and 90^{th} percentile values for 6 variables.

	Parameter/factor values		
Parameters/factors	**Minimum**	**Median**	**Maximum**
Subsoil thickness	50	100	150
LAI	1.5	3.0	4.5
LOS Ks	0.07	1.7	22.75
Subsoil Ks	83.1	194.05	438.4
Peat Storage	α=0.0451 & n=1.2289	α=0.0456 & n=1.1335	α=0.0741 & n=1.0911
Peat Ks	55	141.48	447.3

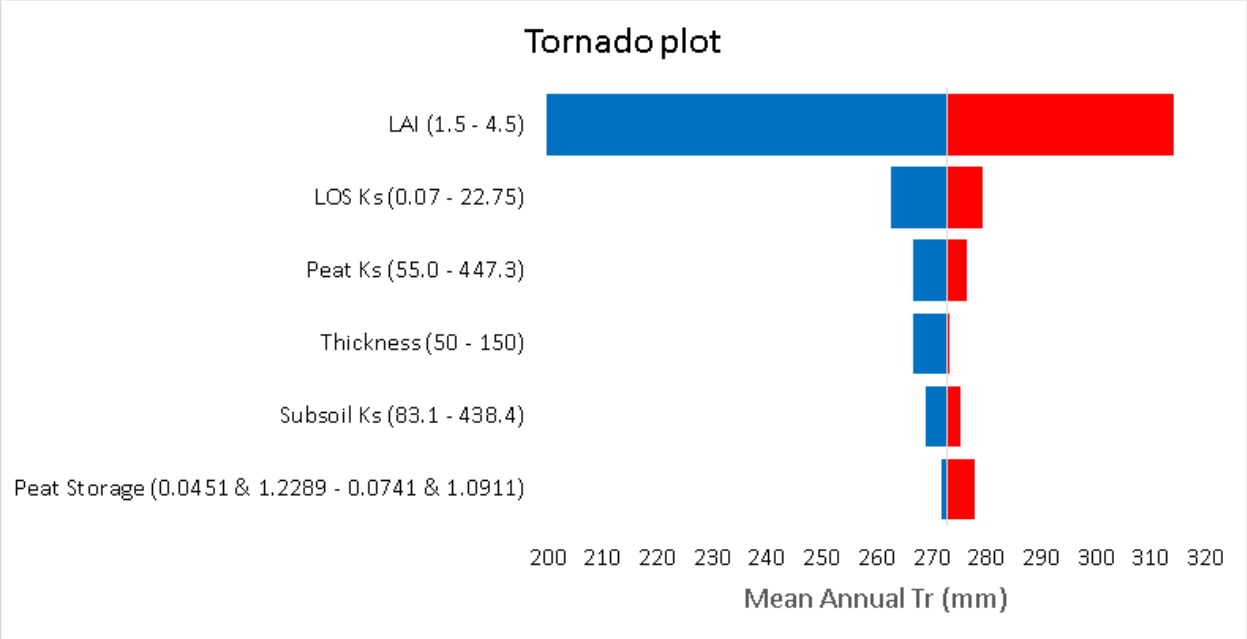

Figure 18. Sensitivity analyses of annual T_r (mean) to 6 variables. Ranges of each simulated variable summarized in Table 4.

3.6 NP frequency distribution and uncertainty for Long-Term Simulation

Fig. 19 shows a typical set of frequency distributions for annual NP values for the same simulation case as that used for Fig. 16 (D100 cover with a LAI value of 3.0). The finer lines represent each individual simulation results (i.e. annual NP distribution for 60 year model) and the heavier lines show the 10^{th}, 50^{th}, and 90^{th} percentiles of the entire frequency distributions. Similar plots of the 10^{th}, 50^{th} and 90^{th} percentiles for annual NP obtained in simulations of the alternative covers for LAI values of 1.5, 3.0, and 4.5 are presented in Fig. 20. These figures illustrate that although LAI has a strong influence on annual NP, there is little variation in the annual NP distribution as a result of changes in subsoil layer thickness.

The sensitivity analyses tornado plot for NP, constructed in a similar manner to that shown previously for T_r (Fig. 18), is shown in Fig. 21. It is clear that LOS K_s was the biggest contributor followed by peat storage and LAI. The subsoil cover thickness only had a modest influence on annual NP.

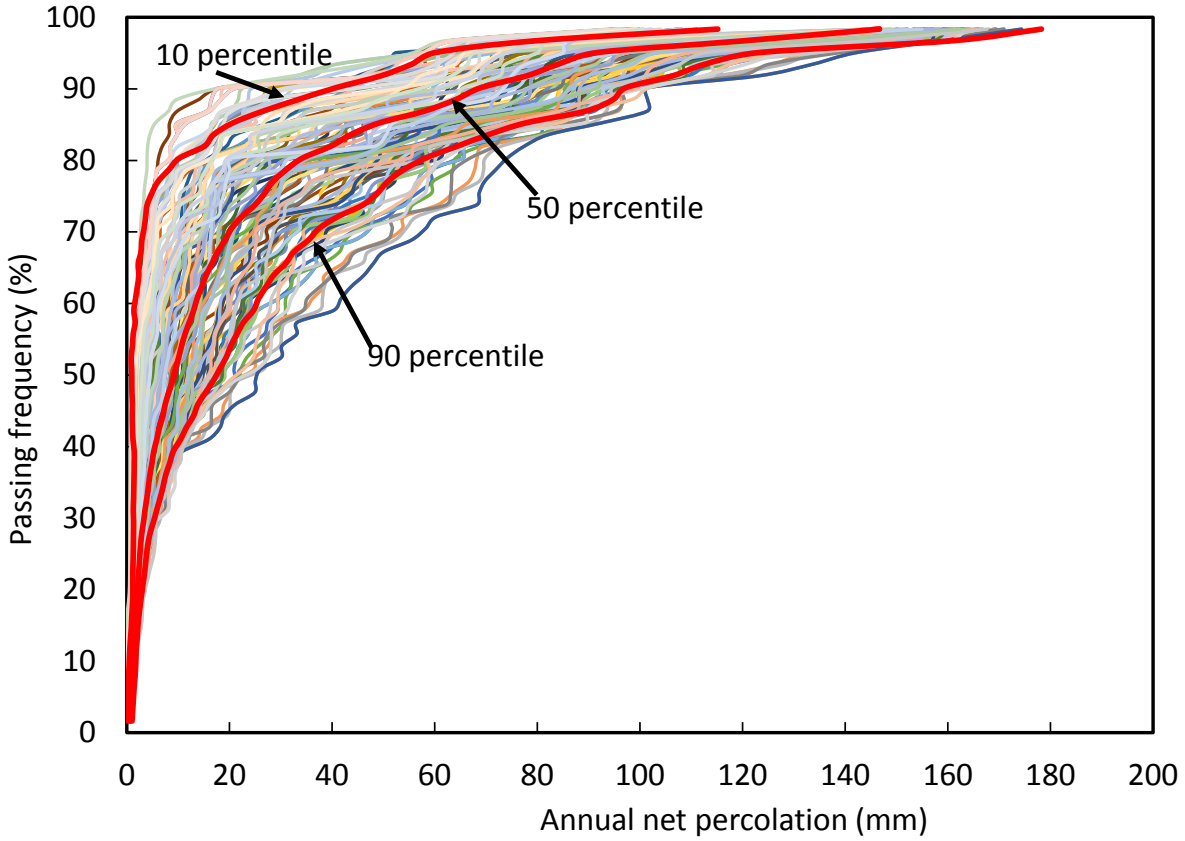

Figure 19. The frequency distribution of annual net percolation (NP) at 135 realizations for the D100 with an LAI of 3.0.

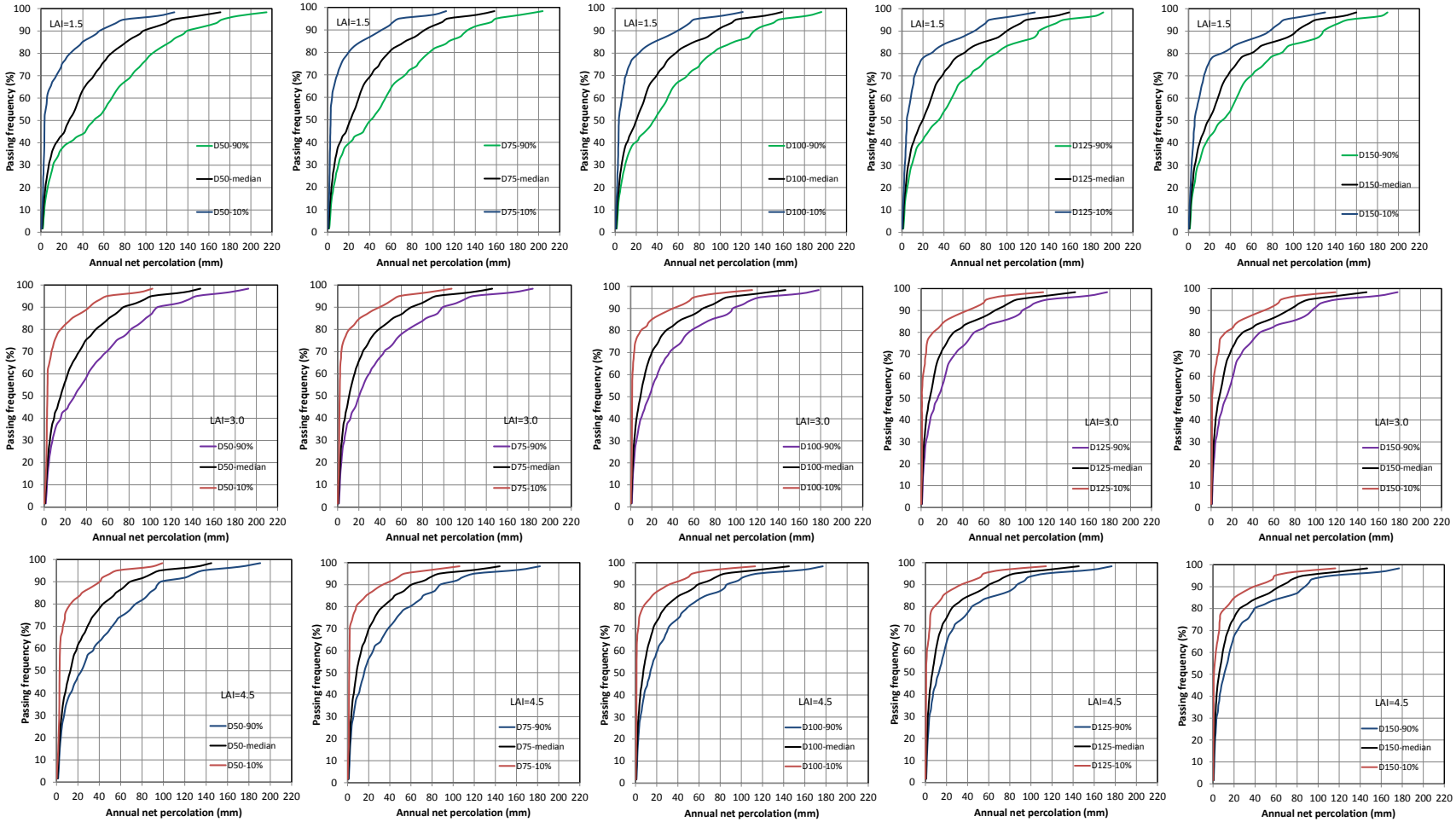

Figure 20. The frequency distributions of annual net percolation at the 10th, 50th, and 90th percentiles for all covers with the LAI=1.5, 3.0, and 4.5. The D50, D75, D100, D125 and D150 represent the subsoil thicknesses of 50, 75, 100, 125 and 150 cm, respectively.

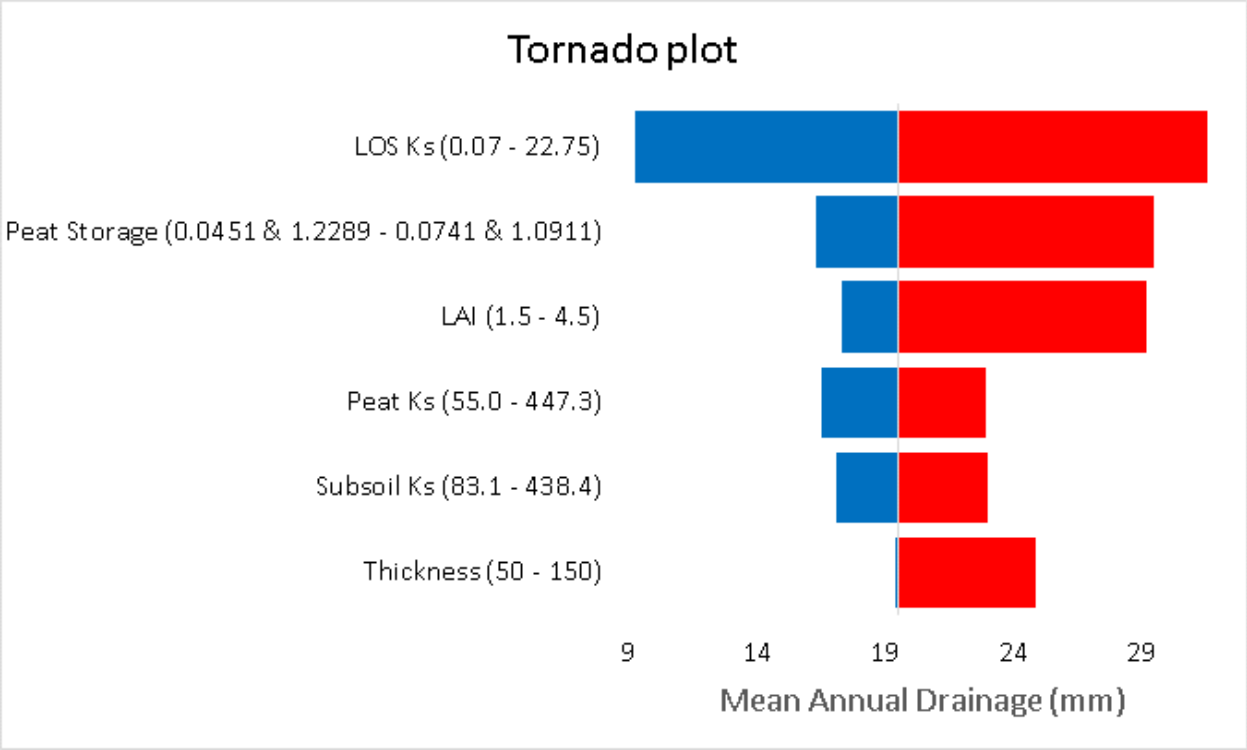

Figure 21. Sensitivity analyses of annual net percolation (mean) to 6 variables.

3.7 Statistics of annual T_r and NP outputs

The statistical summary of the annual values of Tr and NP obtained from the 135 long-term simulations for each alternate cover for the range of LAI values is presented in Tables 5a and 5b, respectively. For the same LAI, the mean of annual T_r did not show a significant increase with increasing subsoil thickness.

Table 5a. Statistics of annual T_r outputs for 135 realizations for each cover with each LAI.

	Cover	No.	Annual T_r (mm)			
			Mean	Standard deviation	Minimum	Maximum
LAI= 1.5						
	D50	60 × 135	192.0	24.6	97.1	235.6
	D75	60 × 135	195.3	25.1	95.5	241.5
	D100	60 × 135	196.5	25.3	94.2	243.3
	D125	60 × 135	196.4	25.4	92.5	244.2
	D150	60 × 135	195.6	25.4	90.8	244.7
LAI=2.0						
	D50	60 × 135	222.9	32.7	111.7	280.2

	D75	60 × 135	226.6	33.4	108.6	287.9
	D100	60 × 135	227.9	33.5	106.9	288.5
	D125	60 × 135	227.6	33.3	104.9	290.2
	D150	60 × 135	226.6	33.0	102.7	291.8
LAI= 2.5						
	D50	60 × 135	247.1	38.8	124.8	315.0
	D75	60 × 135	251.2	39.5	121.1	324.7
	D100	60 × 135	252.4	39.3	118.5	325.8
	D125	60 × 135	252.0	38.8	116.9	325.7
	D150	60 × 135	251.0	38.3	114.4	325.7
LAI=3.0						
	D50	60 × 135	266.8	43.3	137.2	342.6
	D75	60 × 135	271.0	43.8	133.2	354.5
	D100	60 × 135	272.3	43.3	130.1	355.6
	D125	60 × 135	271.9	42.7	128.1	355.0
	D150	60 × 135	270.9	42.1	126.2	353.2
LAI= 3.5						
	D50	60 × 135	283.0	46.6	148.8	364.1
	D75	60 × 135	287.4	46.9	145.0	378.2
	D100	60 × 135	288.6	46.3	141.5	379.4
	D125	60 × 135	288.3	45.5	139.2	378.4
	D150	60 × 135	287.4	44.9	137.4	375.9
LAI= 4.5						
	D50	60 × 135	307.5	51.0	167.9	398.3
	D75	60 × 135	312.0	51.0	164.6	412.4
	D100	60 × 135	313.4	50.1	161.1	414.4
	D125	60 × 135	313.3	49.2	158.5	412.1
	D150	60 × 135	312.6	48.5	156.9	408.3

Table 5b . Statistics of annual net percolation (NP) outputs for 135 realizations for each cover with each LAI.

	Cover	**No.**	**Annual net percolation (mm)**			
			Mean	**Standard deviation**	**Minimum**	**Maximum**
LAI= 1.5						
	D50	60 × 135	36.4	43.2	0	224.5
	D75	60 × 135	33.5	41.7	0	209.7
	D100	60 × 135	33.1	41.4	0	201.7
	D125	60 × 135	33.2	41.4	0	197.1
	D150	60 × 135	33.5	41.4	0	193.2
LAI=2.0						
	D50	60 × 135	32.0	39.9	0	206.8
	D75	60 × 135	28.2	37.7	0	192.7

	D100	60 × 135	27.0	37.1	0	185.5
	D125	60 × 135	26.7	37.0	0	181.3
	D150	60 × 135	26.6	37.1	0	177.5
LAI= 2.5						
	D50	60 × 135	29.5	37.9	0	198.6
	D75	60 × 135	25.2	35.3	0	185.5
	D100	60 × 135	23.6	34.5	0	178.2
	D125	60 × 135	23.1	34.3	0	173.7
	D150	60 × 135	23.0	34.5	0	173.0
LAI=3.0						
	D50	60 × 135	27.9	36.7	0	194.2
	D75	60 × 135	23.4	33.9	0	181.4
	D100	60 × 135	21.6	32.9	0	174.4
	D125	60 × 135	21.0	32.7	0	169.5
	D150	60 × 135	20.9	32.9	0	171.0
LAI= 3.5						
	D50	60 × 135	26.8	35.8	0	191.7
	D75	60 × 135	22.2	32.9	0	179.6
	D100	60 × 135	20.4	31.9	0	173.1
	D125	60 × 135	19.8	31.7	0	167.8
	D150	60 × 135	19.7	32.0	0	167.6
LAI= 4.5						
	D50	60 × 135	25.9	34.9	0	190.0
	D75	60 × 135	20.8	31.9	0	179.1
	D100	60 × 135	19.0	30.9	0	172.8
	D125	60 × 135	18.4	30.7	0	167.3
	D150	60 × 135	18.3	31.0	0	167.4

3.8 Supported LAI range for each cover

In order to evaluate the maximum sustainable LAI for each simulated cover, the median annual T_r for each LAI was plotted against LAI. A second curve, representing the annual T_r (expressed as a mean, maximum, and minimum) required to support a particular value of LAI was then plotted on the same graph. This latter relationship was developed by Huang et al. (2011) and was developed from literature based relationships between LAI, ANPP (above-ground net primary production), and actual evapotranspiration (ET_a). This figure (Fig. 22) was used to estimate a required annual T_r to support the LAI specified in the long-term simulation. The intersection of the curve of annual T_r verses LAI and the required T_r line is designated as the maximum

sustainable LAI. It is important to note that there was no significant change in this value with cover thickness. Overall, the LAI range that can be supported for each cover seems be between 2.5 to 3.0. It is also important to note however, given the uncertainties associated with the relationship between LAI and Tr, as well as the large uncertainty in the thresholds in Fig. 22, the actual LAI for these sites could be much greater than the assumed limit of 2.5-3.

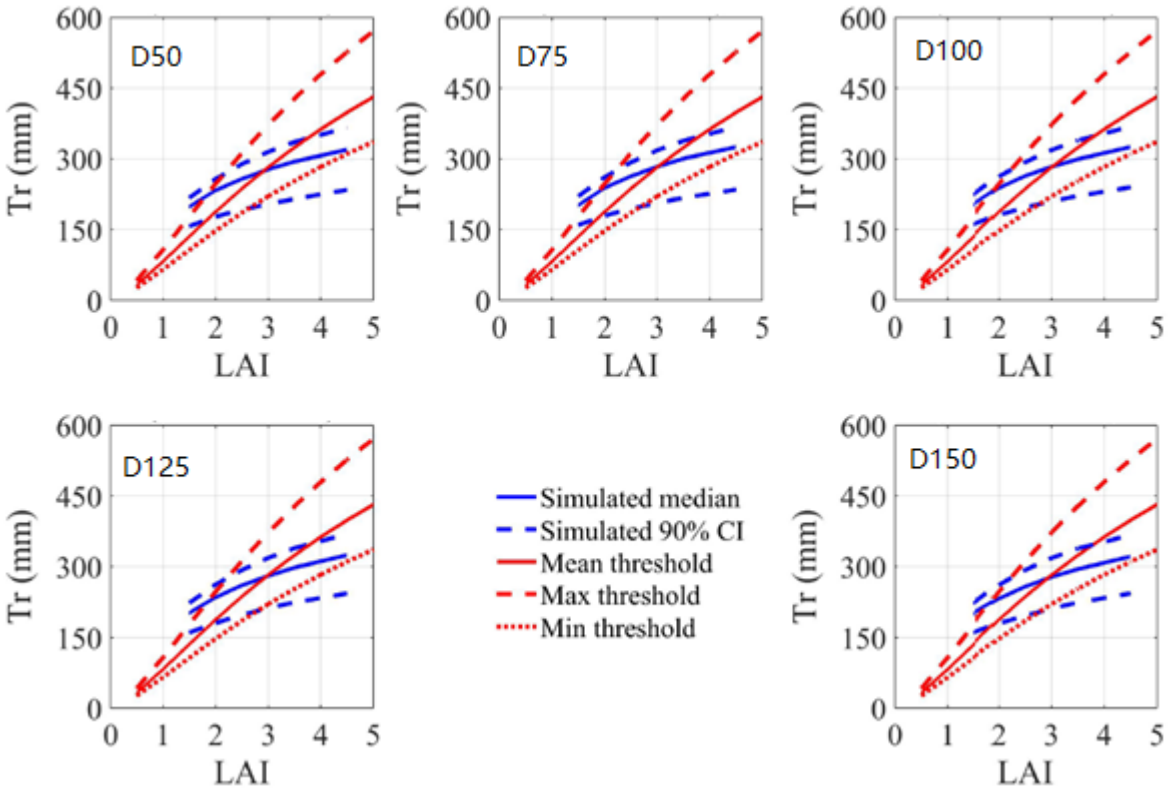

Figure 22. Maximum supported LAI by the simulated annual T_r for each cover.

4. Conclusions and Recommendations

The following conclusions were drawn from the calibration and 60 year climate simulations:

1) The optimization method appeared to provide a reasonable set of hydraulic properties for the various cover soils; however, only the K_s values could be evaluated against independent measurements.

2) The increases in the mean annual T_r and the subsequent decreases in NP, over the 60 year climate cycle as a result of increasing the subsoil thickness from 50 cm to 150 cm, were relatively small. The main reason is that the subsoil is very sandy and has a very low field capacity of approximately 5%. Assuming that the wilting point water content was close to zero, this would mean that the maximum volume of plant available water would only increase by 50 mm for an increase in the thickness of the subsoil of 100 cm.
3) The LOS K_s had the greatest influence on the annual mean T_r and NP. The LOS K_s had a large range of optimized values, from 6.0e-9 to 4.3e-5 m/s (approximately 0.5 to 4000 mm/day). At the low end of this range, the LOS K_s could restrict drainage sufficiently to increase the water availability to plants following a large infiltration event. The use of a simple exponentially decreasing root distribution with depth (Fig. 9) could also under-estimate the importance of this effect. It is also important to note that at the higher values of LOS K_s, the drainage of water from the subsoil is unrestricted and transpiration rates will be limited by available water storage. This is exemplified by the simulated maximum NP values which were as high as 160 to 225 mm annually. Therefore, the reclamation design should consider the effect of spatial variability of LOS hydraulic properties on the performance of reclamation covers.
4) The peat K_s and water storage both played an important, albeit secondary, role in affecting T_r. The higher values of peat K_s did appear to increase soil evaporation and consequently reduce the available water for plant transpiration. This effect might be expected to diminish once an LFH or leaf litter layer gets established. In contrast, the higher range of peat water storage resulted in increased T_r. Restricting the simulations to only one peat thickness (20 cm) did not allow the impact of varying peat thickness to be evaluated. It may be of value to utilize the model to quantify the range of Tr and NP that would develop for a range of peat thickness and peat water storage properties. This may also require more detailed modelling and interpretation of the impact that a thicker peat layer might have on the thermal conditions within the cover.
5) The maximum sustainable level of LAI for each cover alternative ranged from 2.5 to 3.0 based on the simulation and the estimation method used to relate LAI to T_r. This

relationship was assumed from the literature and may not necessarily represent the relationships at ACS.

There are a number of recommended directions for future work that may be considered based on this study. These include the following:

1) Only four of the treatments (a total of 12 cells) with three years of monitoring were evaluated in this study. We would recommend that the most recent year of monitoring data be included and that the hydraulic properties for all 39 cells be optimized with a view to more fully defining the spatial and temporal variability associated with the various material types and cover designs.
2) The temporal uncertainty of hydraulic parameters was included in the overall parameter uncertainty in this study since the hydraulic properties were separately optimized in each of the three years. Although the temporal uncertainty only ranged from 3% for subsoil to 21% for LOS in the overall uncertainty, extending the calibration period for all of the covers may provide more clarity as to whether temporal variations in the hydraulic properties of these soils is occurring.
3) Only unfrozen days were simulated in this study without consideration for the coupling between the energy and water balance. It is recommended that the study be extended to include full coupling of the water and thermal energy balance, with a particular focus on understanding and simulating the time delay in ground thaw and the start of transpiration in the thick peat covers. This approach may also prove to be of value in simulating the dynamics in soil water and temperature over the whole water year, providing better insights into snow melt infiltration and runoff processes associated with spring melt.
4) The results of the 60 year simulations highlighted the potential control over T_r and NP that may be provided by control of the hydraulic properties of the LOS. Further research may want to further evaluate this hypothesis by direct testing of the in situ properties of the LOS and the use of monitoring to establish if 'perched' conditions develop on the LOS surface following large infiltration events.

References

Allen RG, Pereira LS, Raes D, Smith M. 1998. Crop evapotranspiration -Guidelines for computing crop water requirements - FAO Irrigation and drainage paper 56. FAO - Food and Agriculture Organization of the United Nations: Rome.

Bockstette et al. 2016. Personal data exchange, no paper and no report.

Bond-Lamberty, B., S. T. Gower, D. E. Ahl, and P. E. Thornton. 2005. Reimplementation of the BIOME-BGC model to simulate successional change. Tree Physiol. 25:413–424.

Braden, H. 1985. Ein Energiehaushalts- und Verdunstungsmodell for Wasser und Stoffhaushaltsuntersuchungen landwirtschaftlich genutzer Einzugsgebiete. Mittelungen Deutsche Bodenkundliche Geselschaft, 42, 294-299.

Dang, Q. L., H. A. Margolis, M. R. Coyea, M. Sy, and G.J. Collatz. 1997. Regulation of branch-level gas exchange of boreal trees: Roles of shoot water potential and vapor pressure difference. Tree Physiol., 17: 521-535.

Eastman, P.A.K. and E.L. Camm. 1995. Regulation of photosynthesis in interior spruce during water stress: changes in gas exchange and chlorophyll fluorescence. Tree Physiol. **15**: 229–235.

Feddes, R.A., Bresler, E. and Neuman, S. P. 1974. Field test of a modified numerical model for water uptake by root systems. *Water Resources Research* 10: 1199-1206.

Huang, M., S. Lee Barbour, and Sean K. Carey. 2015. The impact of reclamation cover depth on the performance of reclaimed shale overburden at an oil sands mine in Northern Alberta, Canada. Hydrological Processes 29: 2840-2854.

Huang, M., Barbour, L., and Carey, S. 2012. Numerical modelling of the long-term water dynamics and the impact of soil cover depth on transpiration from reclamation soil covers over shale overburden. Report prepared for Syncrude Canada Limited.

Huang, M., Barbour, S.L., Elshorbagy, A., Zettl, J.D., and Si, B.C. 2011. Water availability and forest growth in coarse textured soils. *Canadian Journal of Soil Science* 91, 199-210.

Huang, M., Zettl, J., and Barbour, L. 2011. Preliminary soil-water-atmospheric modeling of the proposed Aurora capping treatments. Report prepared for Syncrude Canada Limited.

Huang, M., Zettl, J. D., Barbour, S. L., and Pratt, D. 2016. Characterizing the spatial variability of the hydraulic conductivity of reclamation soils using air permeability. *Geoderma* 262:285-293.

Kimball, J.S., P.E. Thornton, M.A. White and S.W. Running. 1997. Simulating forest productivity and surface–atmosphere carbon exchange in the BOREAS study region. Tree Physiol. 17:589–599.

Meiers G., Barbour S. L., Qualizza, C. and Dobchuk B. 2011. Evolution of the hydraulic conductivity of reclamation covers over sodic/saline mining overburden. *Journal of Geotechnical and Geoenvironmental Engineering* 137: 968-976.

O'Kane Consultants Inc., 2016. Syncrude Canada Ltd- Aurora Fort Hills north mine soil capping studying-Record of soil moisture and meteorological performance monitoring system installation report. OKC Report No. 690/99-01.

O'Kane Consultants Inc., 2015. Syncrude Canada Ltd- Aurora Fort Hills north mine soil capping studying-Data characteristics and analysis. OKC Report No. 690/115.

O'Kane Consultants Inc., 2014. Aurora soil capping study- annual performance monitoring report. OKC Report No. 690/102-01.

O'Kane Consultants Inc., 2013. Aurora soil capping study of cover system materials characterization program-hydraulic conductivity testing. OKC report No. 690/99-03.

O'Kane Consultants Inc., 2009. PSD reduced data for potential capping study materials.

Pernitsky, T., Hu, W., Si, B.C., Barbour, L. 2016. Effects of petroleum hydrocarbon concentration and bulk density on the hydraulic properties of lean oil sand overburden. *Canadian Journal of Soil Science* 96, 435-446.

Ritchie, J. T. 1972. Model for predicting evaporation from a row crop with incomplete cover, Water Resources Research 8: 1204-1213.

Sigouin, M.J.P., Dyck, M., Si, B.C., Hu, W. 2016. Monitoring soil water content at a heterogeneous oil sand reclamation site using a cosmic-ray soil moisture probe. *Journal of Hydrology* 543,

510-522.

van Dam, J. C., J. Huygen, J. G. Wesseling, R. A. Feddes, P. Kabat, P. E. V. van Walsum, P. Groenendijk, and C. A. van Diepen. 1997. Theory of SWAP version 2.0, *Report 71*, Dept. of Water Resour., Wageningen Agricultural University, Wageningen, the Netherlands.

Van Genuchten, M. T. 1980. A closed-form equation for predicting the hydraulic conductivity of unsaturated soils. Soil Science Society of America Journal 44: 892-898.

Zettl, J., M. Huang, S.L. Barbour. 2014. Hydraulic conductivity testing of the aurora capping treatments. Report to Environmental Research Syncrude Canada Ltd., Canada.